Bulletin of the JSME Vol.20, No.1, 2025
Journal of Fluid Science and Technology

Numerical analysis validating the standard k-epsilon model for the kinetic energy of turbulence subjected to weak but long-lasting wind tunnel blockage acceleration

Akira ONO*, Hiroki SUZUKI*, Toshinori KOUCHI* and Kento TANAKA*
*Graduate School of Environmental, Life, Natural Science and Technology, Okayama University
3-1-1 Tsushima-naka, Kita-ku, Okayama, 700-8530, Japan
E-mail: h.suzuki@okayama-u.ac.jp

Received: 24 December 2024; Revised: 26 February 2025; Accepted: 14 April 2025

Abstract
The aim of this study is to investigate the effect of weak but prolonged mean flow accelerations, such as those observed in wind tunnel blockage acceleration, on free-stream turbulence. Specifically, this research aims to validate a model previously developed based on the k-epsilon model. To test this model, the study focuses on scenarios where the turbulence under acceleration is steady and isotropic, since the model suggests that this type of acceleration has no effect on the turbulent kinetic energy. To examine this suggestion, the turbulence within a periodic box was analyzed using large-eddy simulation (LES) based on the conventional Smagorinsky model framework. The numerical analysis is based on a method that conserves velocity fluctuation intensities. The results show that while high rate of acceleration deviates turbulent kinetic energy, low rate acceleration has hardly any effect on turbulent kinetic energy, enstrophy, pressure fluctuation, relative pressure fluctuation intensity, and higher-order statistics of a velocity fluctuation. These results validate the accuracy of the model proposed in the previous studies. These results were obtained by focusing on differences in Reynolds numbers and the spatial scale of the forcing.

Keywords : Turbulent flows, Large-eddy simulation, Homogeneous turbulence, K-epsilon model, Wind tunnel blockage

1. Introduction

In the field of fluid mechanics, turbulence in incompressible Newtonian fluids, which requires both elucidation and modeling, can generally be divided into turbulence observed near walls and that observed in the free stream (Comte-Bellot and Corrsin, 1971; Mohamed and LaRue, 1990; Lavoie et al., 2007; Kurian and Fransson, 2009; Krogstad and Davidson, 2011). Although this incompressible free-flow turbulence does not involve mean velocity gradients or Reynolds stress contributions in the downstream region, research aimed at elucidating the characteristics of turbulent kinetic energy and its viscous dissipation rate remains active as of the present. For example, the non-equilibrium characteristics of free-stream turbulence (Vassilicos, 2015) have recently received considerable attention in studies using wind tunnel facilities (e.g., Gomes-Fernandes et al., 2012; Valente and Vassilicos, 2012, 2013; Nagata et al., 2013). Accurately reproducing such free-stream turbulence experimentally and validating the accuracy of the reproduced flow and turbulence fields can contribute significantly to the understanding and modeling of free-stream turbulence (e.g., Valente and Vassilicos, 2013; Suzuki et al., 2016), as focused in this study.

One of the differences between studies using wind tunnel experiments and those relying on numerical simulations lies in the potential errors in reproducing flow and turbulence fields. In particular, reproducing a spatially uniform mean flow in wind tunnel experiments may be more challenging than in numerical simulations (Barlow and Rae, 1999). For example, periodic boundary conditions (e.g., de Bruyn Kops and Riley, 1998) are considered difficult to implement grid turbulence experimentally, and there are previous studies have paid considerable attention to ensuring sufficient uniformity of the free stream velocity in the streamwise direction (Suzuki et al., 2016). As boundary layers develop on the wind

Paper No.24-00498
[DOI: 10.1299/jfst.2025jfst0004]

tunnel walls along the streamwise direction, the effective cross-sectional area of the wind tunnel decreases, potentially resulting in a weak but prolonged acceleration of the free stream (de Graaff and Eaton, 2000; Schlatter et al., 2009; Örlü and Schlatter, 2013). This type of acceleration is qualitatively different from the brief contraction-induced acceleration used to enhance the isotropy of grid turbulence reproduced by a static turbulence grid (Comte-Bellot and Corrsin, 1971), or rapidly distorted homogeneous turbulence (Hadžić et al., 2001; Girimaji et al., 2003; Ayyalasomayajula and Warhaft, 2006; Gylfason and Warhaft, 2009; Zusi and Perot, 2013, 2014; Clay and Yeung, 2016; Mugundhan et al., 2020). Previous studies have often used cylinder wakes and bluff bodies to investigate the effects of wind tunnel blockage-induced acceleration on experimentally reproduced flow fields (West and Apelt, 1982; Laneville, 1990; Ota et al., 1994; Choi and Kwon, 1998). On the other hand, the present research focuses on elucidating the effects of wind tunnel blockage-induced acceleration (Suzuki et al., 2016), which is weak but long-lasting, on highly isotropic free-flow turbulence. The magnitude of acceleration covered by this objective appears to be even smaller than that of the previous studies with accelerations smaller than those previously mentioned (Hunt and Carruthers, 1990; Kurian and Fransson, 2007).

This acceleration, which exists as an error in the reproduction of the flow field, should ideally have no effect on the reproduced free-stream turbulence and needs to be validated quantitatively. Therefore, the focus of this study is to address the effects of such a weak but long-lasting mean flow acceleration, caused by wind tunnel blockage, on the characteristics of free-stream turbulence. Previous studies have used the standard k-epsilon model (Pope, 2000) to quantify the influence of this type of acceleration on statistics of free-stream turbulence (Suzuki et al., 2016, 2018), specifically examining its effects on turbulent kinetic energy and its viscous dissipation rate. As a result, the effect of streamwise acceleration on the decay characteristics of grid turbulence was evaluated, with the decay characteristics being studied in detail. The modeling approach, which replicates the numerical results from the governing equations of the k-epsilon model, has been established as a numerically based theoretical analysis. The scope of this modeling is determined by the time-integrated acceleration rate of the mean flow (Suzuki et al., 2018), and an extended version of the modeling equation has also been developed (Suzuki et al., 2020a).

The model developed in the previous studies to describe the effects of wind tunnel blockage-induced acceleration on free-flow turbulence has yet to be validated by unsteady turbulence analysis. The k-epsilon model underlying this model derives the eddy viscosity from turbulent kinetic energy and dissipation rate using dimensional analysis, which results in the loss of spatial scale aspects of the turbulence. Based on these points, there is a need to validate this numerical prediction model. Although previous studies have explored the application range of this prediction model (Suzuki et al., 2018, 2020a), they have focused more on the time integral of the acceleration rate rather than the acceleration rate itself. Focusing only on the time-integrated acceleration rate fails to distinguish the effects of strong acceleration over a short period from those of weak acceleration over a long period on free-stream turbulence. Since the acceleration induced by the wind tunnel blockage corresponds to the case of weak acceleration, the effects of weak, prolonged acceleration on free stream turbulence should be investigated. The model asserts that turbulent kinetic energy is completely unaffected by acceleration if the turbulence under this type of acceleration is steady and isotropic. This assertion is considered to be quite straightforward and can be effectively validated by unsteady analysis in this study.

The aim of this study is to examine this k-epsilon-based model suggestion that describes the effect of wind tunnel blockage-induced acceleration on turbulent kinetic energy using steady turbulence subjected to weak but long-lasting mean flow acceleration. To address this issue, the steady turbulence is reproduced within a three-dimensional periodic cubic computational domain under the influence of mean flow acceleration and analyzed using large-eddy simulation (LES). The governing equations to be analyzed are formulated for the fluctuating flow as deviations from the mean flow. The mean flow used in this study is identical to that assumed by the model equation to be validated and is axisymmetric with respect to the direction of acceleration. The analytical method is based on a high-order central difference scheme with sufficient accuracy in conserving velocity fluctuation intensities. The results obtained in this study indicate that when the mean flow acceleration rate is low, the turbulent kinetic energy remains unaffected by the acceleration, as predicted by the model. Conversely, when the acceleration rate is not sufficiently low, the turbulent kinetic energy is significantly affected. These results are further examined from the perspective of turbulence statistics in the turbulence affected by the acceleration. Finally, the conclusions of this study are summarized.

2. Methods

This study investigates a previously proposed model that captures the effect of wind tunnel blockage acceleration on turbulence (Suzuki et al., 2016). This model, based on the k-epsilon turbulence model, describes the influence of

[DOI: 10.1299/jfst.2025jfst0004]

wind tunnel blockage acceleration on turbulent kinetic energy k. Specifically, the effects of fluid acceleration due to wind tunnel blockage on this statistics are expressed as a non-dimensionanl influence function, f, which represents the relative influence on the power law of turbulent kinetic energy:

$$k(t) = k_{\mathrm{o}}\, f(t)\, t^{-n} \tag{1}$$

where t is the non-dimensional time, k_{o} is decay coefficient, and n is the decay exponent in the absence of acceleration. This non-dimensional time is obtained, for example, in a grid turbulence experiment, by non-dimensionalizing real time with respect to the freestream velocity and mesh width (Suzuki et al., 2016). Furthermore, following the previous study (Suzuki et al., 2018), the governing equations of the k-epsilon model yield an equation for the influence function $f(t)$, the solution of which is given by

$$f(t) = \exp(P_{\mathrm{o}} S t) - \frac{3n}{3n-1}\left[\exp(P_{\mathrm{o}} S t) - \exp(C_2 S t)\right],\ C_2 = bC_1 + \frac{C_{\epsilon 1}+5}{6}P_{\mathrm{o}},\ C_1 = -\frac{C_{\epsilon 1}-1}{2}P_{\mathrm{o}}. \tag{2}$$

In this solution, S represents the nondimensional acceleration rate, defined as

$$S = \frac{dU'/dx'}{U_{\mathrm{o}}/D}. \tag{3}$$

Here, U', x' are dimensional quantities of streamwise velocity and accelerated direction, respectively. Also, U_{o} and D present characteristic quantities of velocity and length scales of the bulk flow. In addition, $C_{\epsilon 1}$ is a model constant of the k-epsilon model, and the production term P_{o} is expressed as follows:

$$P_{\mathrm{o}} = \frac{2(a-1)}{1+2a} \tag{4}$$

Here, a is a parameter that characterizes anisotropy value of the turbulence and is defined as follows:

$$a = \frac{\langle v^2\rangle}{\langle u^2\rangle} = \frac{\langle w^2\rangle}{\langle u^2\rangle} \tag{5}$$

Here, u, v, w denotes velocity fluctuations for x, y, z directions, respectively. Also, $\langle\ \rangle$ denotes ensemble average. This influence function $f(t)$ is equal to unity in the absence of wind tunnel blockage acceleration, where $S = 0$.

The characteristics of the model equation under the condition of steady turbulence are investigated, focusing on the model equation for turbulent kinetic energy. The steady state condition of the turbulent kinetic energy in the absence of acceleration corresponds to the case where the decay exponent n in the equation is zero. In this condition, the influence function, which represents the effect of the wind tunnel blockage acceleration on the turbulent kinetic energy, is reduced to the following equation:

$$f(t) = \exp(P_{\mathrm{o}} S t). \tag{6}$$

As shown, when the turbulence is steady, the influence function equation is described by three quantities: the anisotropy of the turbulence a through the form of P_{o}, the non-dimensional acceleration rate S, and the non-dimensional time t. This study also focuses on the case where the turbulence remains isotropic despite the presence of wind tunnel blockage acceleration. When the turbulence is still isotropic, the value of a becomes unity and the value of the production term P_{o} becomes zero. Consequently, the influence function is reduced to the following expression

$$f(t) = 1 \tag{7}$$

This suggests that even in the presence of wind tunnel blockage acceleration, the turbulent kinetic energy is not affected by the acceleration if the influenced turbulence is assumed to be steady and isotropic. The main purpose of this study is to examine this derived result.

2.1. Details of the numerical simulation

The analysis uses a cubic domain with a side length of 2π. Periodic boundary conditions are applied to all sides of the domain. In the absence of acceleration, the analysis is set up to generate steady turbulence within this periodic box. The present study uses this computational domain to assume a localized turbulent field in this study. The origin of this computational domain is aligned with that of the coordinate system, with the x, y, and z directions defined accordingly, where $(x, y, z) = (x_1, x_2, x_3)$. In this analysis, the mean flow velocity field U_i for x_i directions with $i = 1, 2, 3$, which includes the weak acceleration of the fluid due to the wind tunnel blockage, is prescribed in the following form:

$$U_1 = S\, x_1,\ U_2 = -(S/2)\, x_2,\ U_3 = -(S/2)\, x_3. \tag{8}$$

[DOI: 10.1299/jfst.2025jfst0004]

The physical meaning of S can be clarified by considering the following definition of S (Kashiwagi et al., 2022).

$$S = K_o \mathrm{Re},\ K_o = \frac{\nu}{U_o^2}\frac{dU'}{dx'},\ \mathrm{Re} = \frac{U_o D}{\nu}. \tag{9}$$

This mean velocity field satisfies the continuity equation of mean flow. As shown in the above equations, our study considers an axisymmetric mean flow with the x direction as the principal axis. Using this flow as an accelerated flow, the above flow can be transformed into a decelerated mean flow by assigning a negative sign to S.

In this analysis, the governing equations are set up to investigate the effect of the aforementioned mean flow acceleration on the turbulent field. Specifically, the instantaneous components are decomposed into those of mean and fluctuating flows, and the governing equations are specified to analyze the fluctuating components. The governing equations analyzed in this study consist of the continuity equation and the Navier-Stokes equation for the fluctuating components, which are given as follows:

$$\frac{\partial u_i}{\partial x_i} = 0 \text{ and } \frac{\partial u_i}{\partial t} + u_j\frac{\partial u_i}{\partial x_j} = -\frac{\partial p}{\partial x_i} + \frac{1}{\mathrm{Re}}\frac{\partial^2 u_i}{\partial x_j \partial x_j} + f_i + F_i. \tag{10}$$

Here, f_i represents the term resulting from the mean flux for the x_i direction, which is expressed as follows

$$f_1 = -S\,x_1\frac{\partial u_1}{\partial x_1} - S\,u_1,\ f_2 = (S/2)\,x_2\frac{\partial u_2}{\partial x_2} + (S/2)u_2,\ f_3 = (S/2)\,x_3\frac{\partial u_3}{\partial x_3} + (S/2)u_3. \tag{11}$$

This term is specified by the acceleration rate S. In addition, the external force term includes a forcing term that maintains the turbulence at steady state. Based on previous studies (Goto and Vassilicos, 2015; Hirabayashi et al., 2023), this forcing term is expressed according to the linear forcing method as follows

$$F_1 = \frac{2c}{\sqrt{3}}\cos(Mx_2)\cos(Mx_3),\ F_2 = \frac{2c}{\sqrt{3}}\cos(Mx_3)\cos(Mx_1),\ F_3 = \frac{2c}{\sqrt{3}}\cos(Mx_1)\cos(Mx_2) \tag{12}$$

The constant c is the external forcing coefficient, which is set to $c = 0.133$ based on previous research (Rosales and Meneveau, 2005). Also, M is an integer parameter that determines the spatial scale of the forcing, and in this study the value of M is varied around $M = 4$ based on the previous study (Goto and Vassilicos, 2015).

In this study, the above governing equations are analyzed using large-eddy simulation (LES). Therefore, the filtered versions of these equations are solved in this analysis. For the subgrid scale (SGS) model within the LES equations, the Smagorinsky model, which is widely used in such simulations, is employed in this study. The fractional step method is used to solve the system of governing equations. For the spatial discretization, the fourth-order central difference Morinishi scheme is applied (Morinishi et al., 1998; Suzuki et al., 2013a, 2013b). In this study, the skew-symmetric form is used, which inherently conserves the intensities of velocity fluctuations. The viscous terms are discretized using the same scheme as the convective and pressure terms. A previous study (Honda et al., 2021) has pointed out that the conservation accuracy of the velocity fluctuation intensities in the discretized governing equations may affect that of the pressure fluctuation analysis. In order to improve the conservation characteristics of the velocity fluctuation intensities, a six-stage, fourth-order accurate Runge-Kutta method with low storage is used for time integration (Suzuki et al., 2020b). The coefficients of this time integration method are adjusted to minimize the numerical dissipation associated with time integration, which is treated as a conservation error due to the explicit nature of Morinishi's scheme. The study imposes the assumption of periodic boundary conditions on both the velocity field and the pressure field, which leads to the direct solution of the Poisson equation via three-dimensional fast Fourier transforms. Additionally, the Morinishi scheme is employed to discretize the pressure term and the Poisson equation, ensuring the conservation properties of the scheme are maintained. As a result, the kinetic energy conservation error in an inviscid state is also of the order of double precision machine zero. Similarly, the error in the continuity equation is of the order of machine zero in this analysis.

[DOI: 10.1299/jfst.2025jfst0004]

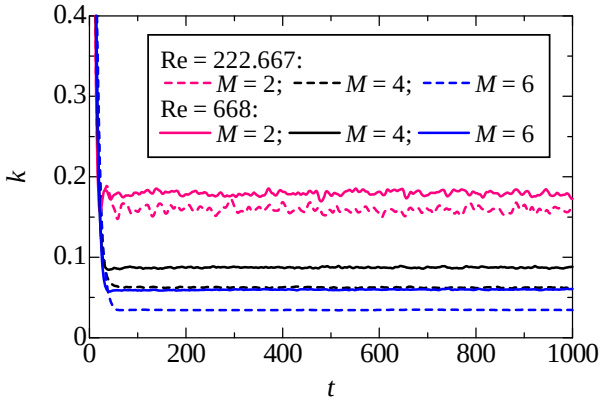

Fig. 1 Time series of turbulent kinetic energy in a steady turbulent flow, unaffected by the acceleration of the wind tunnel blockage. The turbulent kinetic energy converges to a steady value at time $t = 100$. For all values of M, the turbulent kinetic energy increases with the Reynolds number.

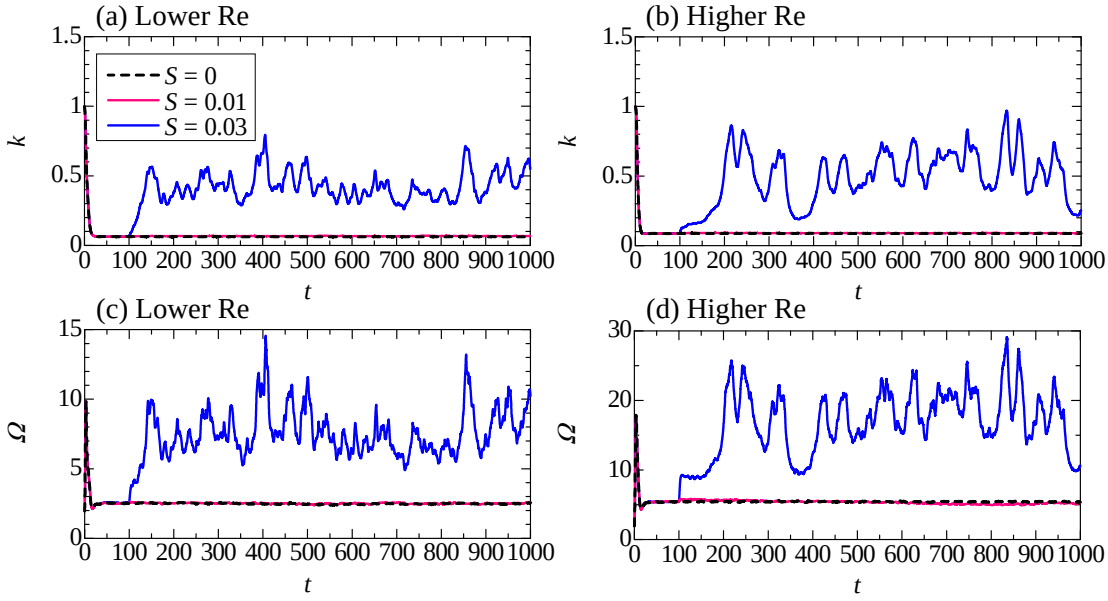

Fig. 2 Time series of turbulent kinetic energy and enstrophy in box turbulence under the influence of wind tunnel blocking acceleration. The results are shown for $M = 4$. Data are shown for two acceleration rates and two Reynolds number conditions, where S is the acceleration rate.The time series of turbulent kinetic energy for $S = 0.03$ differs significantly from that for $S = 0$, while for $S = 0.01$ it is close to the $S = 0$ case. Similar results are observed for the enstrophy.

For the analysis conditions in this study, a uniformly spaced staggered grid with a grid resolution of 32^3 was used as shown in the appendix. Here, this number of grid points is often used in LES analyses of turbulence in a three-dimensional periodic cubic domain, as exemplified by Kobayashi (2005). The time integration conditions were set to a time step Δt of $\Delta t = 0.005$. The Smagorinsky model constant C_s was set to the commonly used value of $C_s = 0.1$. The bulk Reynolds number Re was set to a baseline value of Re = 222.667 based on previous study (Rosales and Meneveau, 2005), and simulations were also performed at a higher Reynolds number of Re = 668, which is three times the baseline value. The acceleration rate S was set to a baseline value of $S = 0.01$, which is larger and more convenient than the acceleration rate measured by our group in the main flow direction of multi-scale grid-generated turbulence. In this study, four conditions were set for the acceleration rate: $S = 0$ for the case without wind tunnel blockage acceleration, $S = 0.01$ as the base value for acceleration, and two additional values, $S = 0.003$ and $S = 0.03$, corresponding to 0.3 and 3 times the baseline value, respectively. The phenomenon of the weak acceleration can be associated with wind tunnel blockage acceleration in experimental facilities. In determining the value of this parameter in the present study, the current wind tunnel experimental data as well as the results from the previous study (Suzuki et al., 2016) conducted by the present

[DOI: 10.1299/jfst.2025jfst0004]

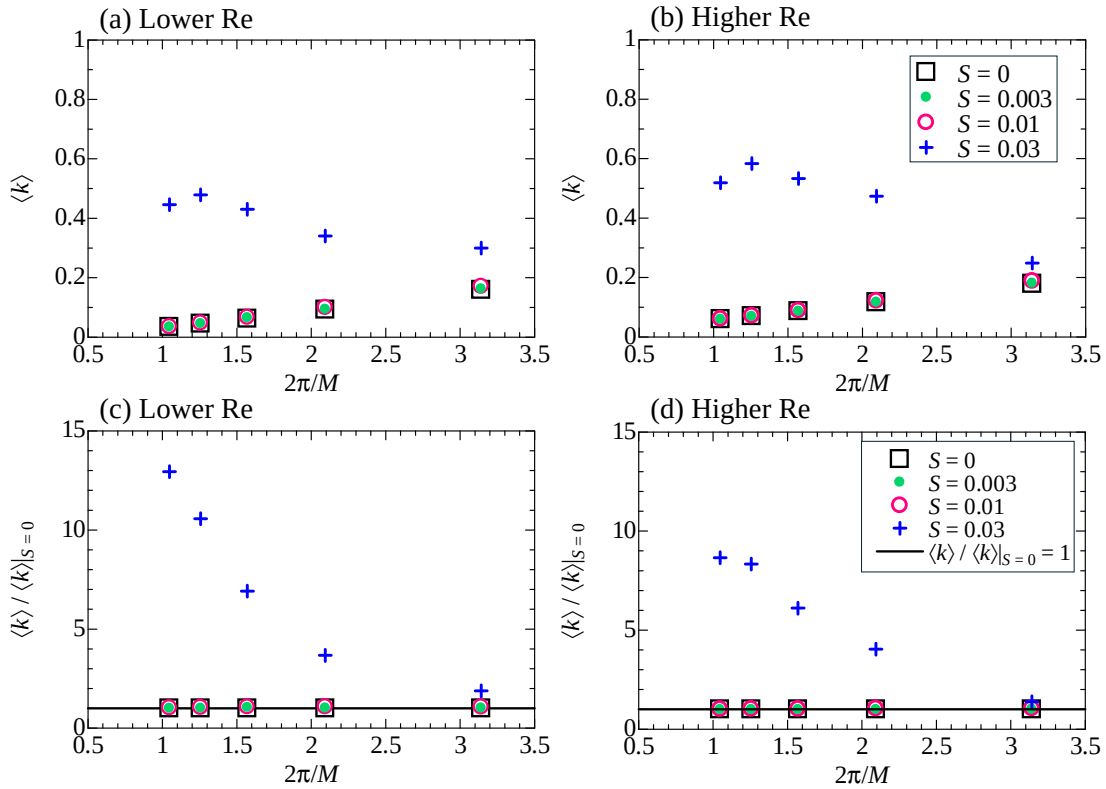

Fig. 3 Mean turbulent kinetic energy as a function of $2\pi/M$ for two Reynolds number conditions. (a) and (b) show the mean values themselves. (c) and (d) show the mean values relative to those for the no-acceleration condition ($S = 0$). For both Reynolds number conditions, the mean value for $S = 0.03$ deviates from that for $S = 0$. This deviation decreases with the increase in $2\pi/M$ due to the decrease in M. In contrast, for acceleration rates below $S = 0.01$, the mean values are close to those for $S = 0$.

group were employed. When the test-section width is designated as the characteristic length scale for the bulk flow, the aforementioned experiment has reported values of this parameter ranging from 1×10^{-3} to 5×10^{-3}. In contrast, the current wind tunnel at Okayama University, utilized by our group, has yielded values approximately from 6×10^{-3} to 8×10^{-3}. The discrepancy between these values can be attributed to the adjustment of the tunnel sidewalls to maintain a constant effective cross-sectional area in the previous experiment. This research employs the setting of 0.01 for the parameter S, which exceeds these reported values. In addition, the spatial scale of the forcing used to generate steady turbulence was varied using the integer coefficient M, with values of $M = 2, 3, 4, 5$, and 6.

3. Results and discussion

3.1. Examining turbulence model predictions

Figure 1 first shows the time series of the turbulent kinetic energy k in the case without acceleration of the free stream. Here, the turbulent kinetic energy is obtained by spatially averaging at each time, but varies with time. The instantaneous turbulent kinetic energy is obtained as follows: $k = (1/2)(u_1^2 + u_2^2 + u_3^2)$. These time series are presented as a function of the parameter M and the Reynolds number Re. In the figure, while the turbulent kinetic energy initially varies with time, it converges to a steady state value at $t = 100$. This result indicates that the generated turbulence can be considered statistically steady at $t = 100$. The steady state value of the turbulent kinetic energy varies as a function of the spatial forcing parameter M, with the steady state value decreasing as M increases. In addition, the steady-state values differ between the two Reynolds number values, with higher turbulent kinetic energy observed at the higher Reynolds number.

Time series of turbulent kinetic energy k and enstrophy Ω under the influence of mean flow acceleration for $M = 4$ are shown in Fig. 2 for both Reynolds numbers. Here the enstrophy Ω is obtained as follows: $\Omega = (1/2)(\omega_1^2 + \omega_2^2 + \omega_3^2)$, where ω_i is a voticity component for the x_i direction. The mean flow acceleration is still applied from $t = 100$. These results are presented with the acceleration rate S as a variable. It is observed that the turbulent kinetic energy remains constant over time for both Reynolds number conditions. Furthermore, for $S = 0.01$, the turbulent kinetic energy is not affected by the acceleration. However, in the case of $S = 0.03$, it is evident that the turbulent kinetic energy increases due

[DOI: 10.1299/jfst.2025jfst0004]

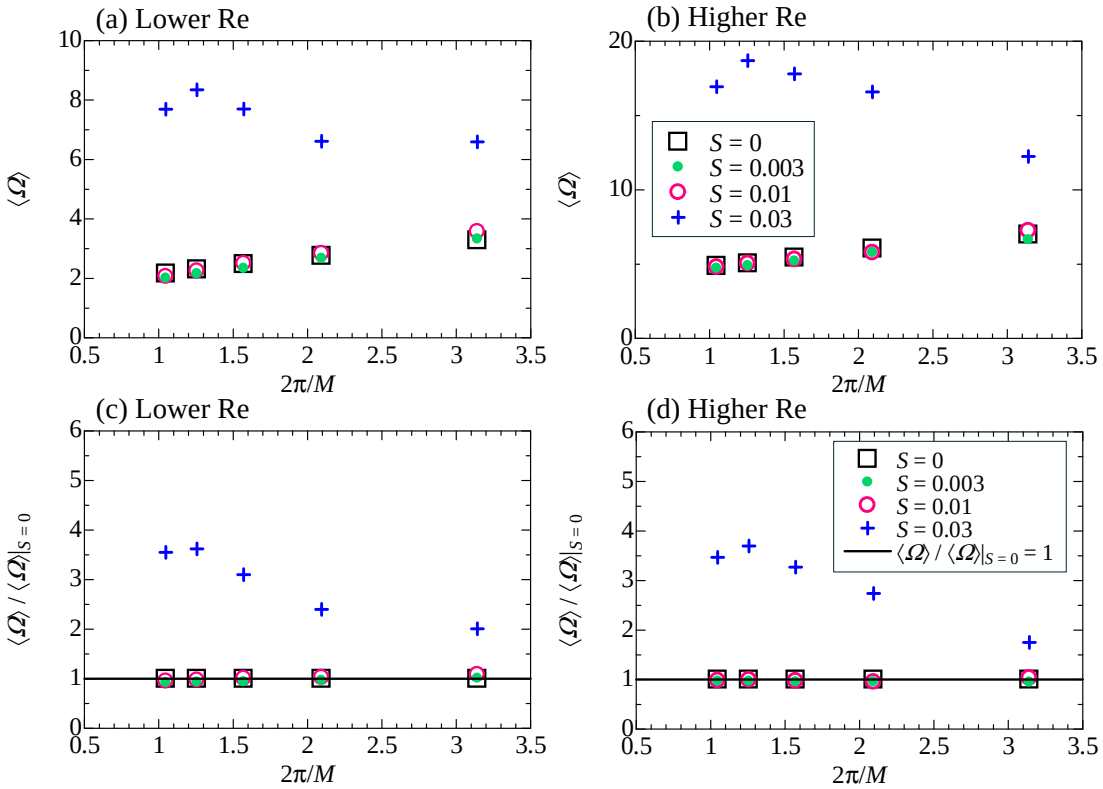

Fig. 4 Dependence of the mean enstrophy values on $2\pi/M$ for $M = 4$. (a) and (b) show the mean values, while (c) and (d) show the values relative to those for $S = 0$. Similar to the results for turbulent kinetic energy, the mean enstrophy affected by acceleration at $S = 0.03$ differs from that for $S = 0$, while the values for $S = 0.01$ are close to those for $S = 0$.

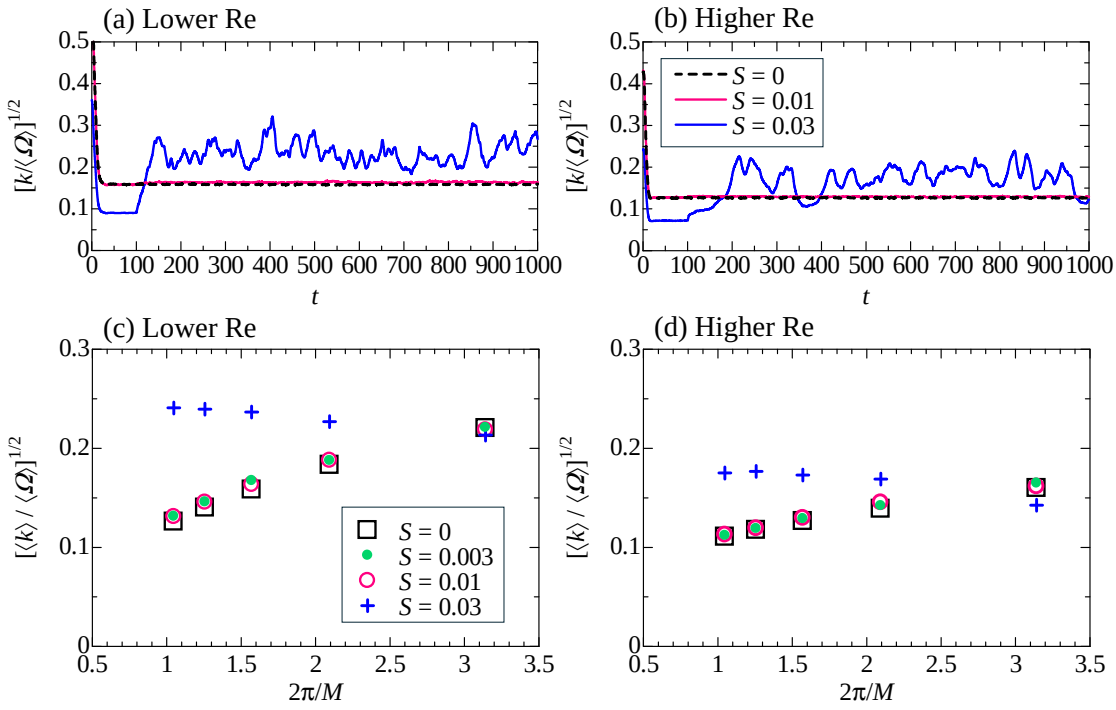

Fig. 5 Dependence of the length scale on the acceleration rate S. (a) and (b) show the time series of the length scale as a function of the acceleration rate for $M = 4$. The time series of the length scale for $S = 0.01$ closely matches that for $S = 0$, and this agreement is observed for both Reynolds number conditions. (c) and (d) show the mean length scale as a function of $2\pi/M$. As $2\pi/M$ decreases with increasing M, the difference between the values for $S = 0.01$ and $S = 0.03$ increases.

[DOI: 10.1299/jfst.2025jfst0004]

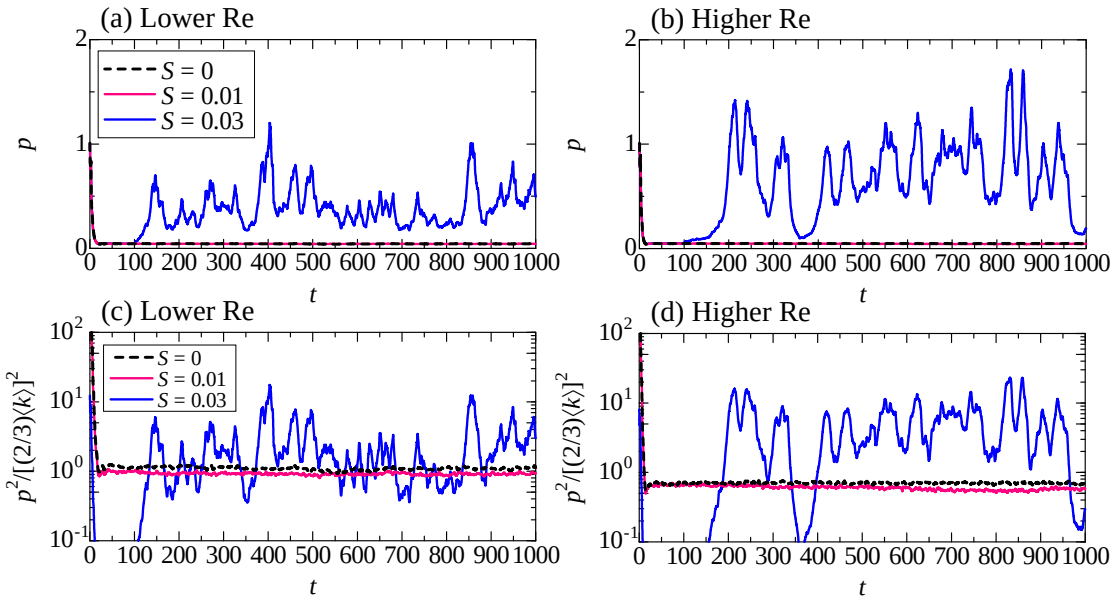

Fig. 6 Effect of acceleration on static pressure fluctuations. (a) and (b) show the effect of acceleration on the time series of static pressure fluctuations, p, for $M = 4$. These static pressure fluctuations are spatially averaged at each instant. (c) and (d) show the effect of acceleration on the time series of relative static pressure fluctuations, where the relative static pressure fluctuations are derived using the mean turbulent kinetic energy.

to the effect of acceleration. The time series of the enstrophy under the influence of the mean flow acceleration is also shown. As shown in the figure, similar to the turbulent kinetic energy, the enstrophy is not affected by the acceleration at $S = 0.01$, while it increases under the influence of $S = 0.03$. The enstrophy reflects the properties of the smaller scale turbulence compared to the turbulent kinetic energy. These results indicate that not only the large-scale turbulence represented by turbulent kinetic energy, but also the small-scale turbulence reflected by enstrophy are unaffected by the mean flow acceleration at $S = 0.01$.

Figure 3 (a) and (b) show the time-averaged turbulent kinetic energy $\langle k \rangle$ as a function of spatial scale $2\pi/M$ for low and high Reynolds number conditions, respectively. The time averaging $\langle\ \rangle$ is taken from $t = 200$ onwards. For the low Reynolds number case shown in (a), free-stream acceleration with an acceleration rate up to $S = 0.01$ has a negligible effect on the mean turbulent kinetic energy. However, when the acceleration rate is $S = 0.03$, the mean flow acceleration increases the mean turbulent kinetic energy, causing it to deviate from the value observed in the absence of acceleration. These results are similarly observed in the high Reynolds number case shown in (b). Figure 3 (c) and (d) show the normalized mean turbulent kinetic energy as a function of spatial scale, where the normalization is performed with respect to the value in the absence of acceleration. If the mean value is unaffected by acceleration, the normalized value would be exactly unity. As shown in both figures, under the influence of acceleration $S = 0.03$, the normalized mean value increases as M increases and the spatial scale $2\pi/M$ decreases. On the other hand, this study again observes that acceleration up to $S = 0.01$ has virtually no effect on the mean values, regardless of the spatial scale.

Figure 4 (a) and (b) show the effects of acceleration on the time-averaged enstrophy $\langle \Omega \rangle$ as a function of spatial scale for low and high Reynolds number conditions, respectively. Similar to the effect on the mean turbulent kinetic energy, acceleration up to $S = 0.01$ has virtually no effect on the mean enstrophy. However, at an acceleration rate of $S = 0.03$, the acceleration increases the mean enstrophy, causing it to deviate from the value observed without acceleration. These results are observed for both Reynolds number conditions. Figure 4 (c) and (d) show the normalized mean values of the enstrophy, using the enstrophy in the absence of acceleration as a reference, plotted as a function of the spatial scale $2\pi/M$. As shown in the figures, acceleration up to $S = 0.01$ does not affect the mean value of the enstrophy, while acceleration at $S = 0.03$ causes it to deviate from unity.

Using turbulent kinetic energy and enstrophy, a length scale can be defined as follows $\sqrt{k/\Omega}$. The time series of this length scale for $M = 4$ are shown in Fig. 5 (a) and (b). In this study, the denominator of this length scale is taken as the mean value of the enstrophy, while the numerator is an instantaneous quantity at each instant. As shown in the figure, for

[DOI: 10.1299/jfst.2025jfst0004]

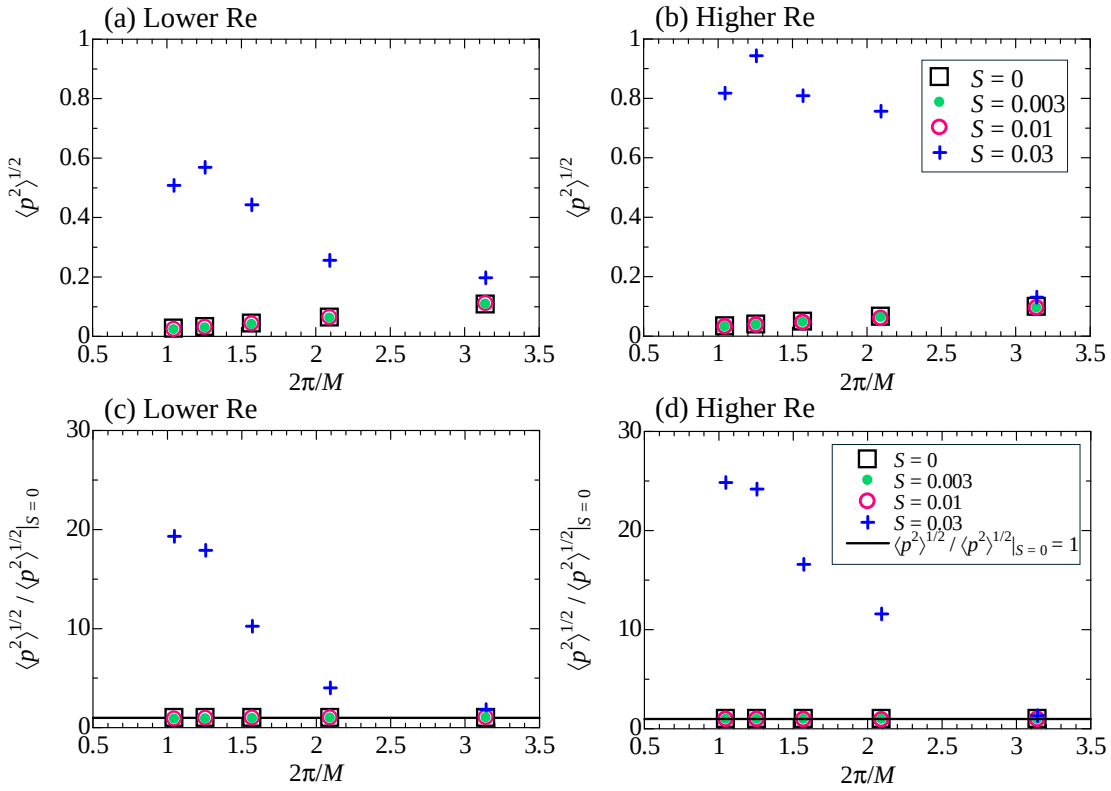

Fig. 7 RMS value of static pressure fluctuation as a function of $2\pi/M$. (a) and (b) show the RMS values for each Reynolds number condition. (c) and (d) show the RMS values relative to those for $S = 0$. Similar to the results for turbulent kinetic energy and enstrophy, the effect of acceleration on the RMS value of the static pressure fluctuation is not observed for $S = 0.01$, but is significantly noticeable for $S = 0.03$. Also, the effect of acceleration on the RMS value of static pressure fluctuations increases with the decrease in $2\pi/M$ due to the increase in M.

an acceleration rate of $S = 0.01$, which is sufficiently small to not affect the turbulent kinetic energy, the time series of this length scale also closely matches that obtained without acceleration. This agreement is observed for both Reynolds number conditions. On the other hand, the acceleration rate of $S = 0.03$ significantly affects the time series of the length scale, causing it to deviate from the unaccelerated case. Figure 5 (c) and (d) show the mean values of the length scale, where the numerator is taken as the mean turbulent kinetic energy, plotted as a function of spatial scale. As shown, in the absence of acceleration, the length scale increases with increasing spatial scale. Under the influence of acceleration up to $S = 0.01$, the length scale remains well aligned with that of the unaccelerated case.

The length scale shown in Fig. 5 is derived from the ratio of turbulent kinetic energy to enstrophy. In this work, the size of the primary turbulent structure is treated as being characterized by $2\pi/M$. However, for values of $S = 0.03$ and similarly large values of M, the length scale no longer scales with $2\pi/M$, however remains nearly constant. As shown in Fig. 3(a)-(b) and Fig. 4 (a)-(b), for cases where the acceleration rate S takes the large value and the forcing parameter M also has a large value, both the turbulent kinetic energy and the enstrophy remain nearly constant instead of scaling with the parameter. This behavior is likely related to the settings in Eq. (10) of this study, which indicate that the forcing term remains constant for any value of the parameter. From these results, we infer a qualitative difference in how strongly the turbulence is constrained to the eddy size of nonequilibrium turbulence depending on whether the forcing on the flow does not vary with time or not. The previous study (Goto and Vassilicos, 2015) reported that the turbulent kinetic energy can still exhibit unsteady fluctuations, highlighting the phenomena of non-equilibrium turbulence, even when the forcing on the flow remains steady over time. As shown in Fig. 2, in this study, unsteady fluctuations in the turbulent kinetic energy were observed when the acceleration rate was large. In these cases, the turbulent kinetic energy can fluctuate unsteadily, making the flow less constrained by the eddy size of $2\pi/M$. As a result, the flow appears to maintain a turbulent kinetic energy level that is more consistent with the magnitude of the forcing term in the governing equations.

In this study, in addition to turbulent kinetic energy and enstrophy, we also investigate the effect of acceleration on box turbulence from the perspective of a static pressure fluctuation. Figure 6 (a) and (b) show the time series of the static

[DOI: 10.1299/jfst.2025jfst0004]

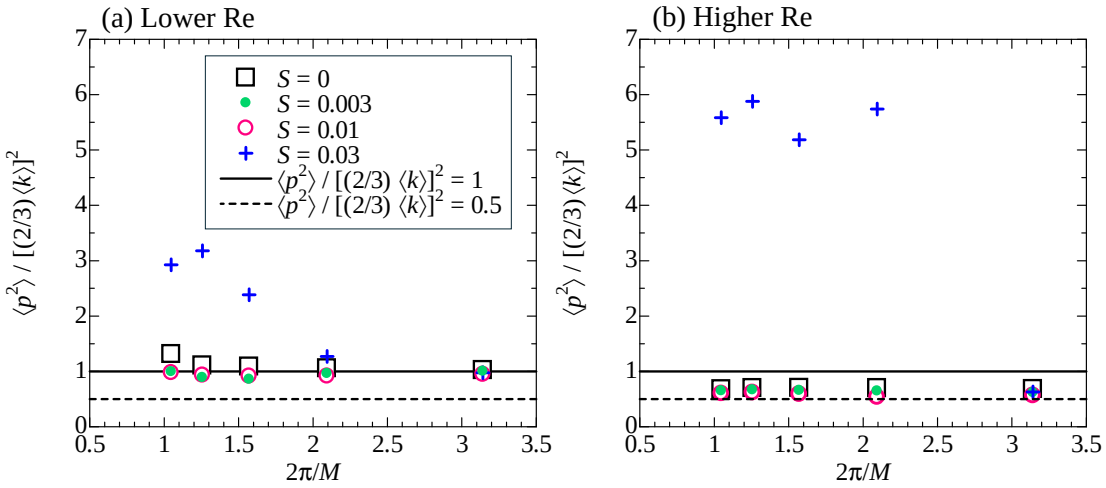

Fig. 8 Relative intensity of static pressure fluctuation as a function of $2\pi/M$. (a) and (b) show results for low and high Reynolds number conditions. Acceleration at $S = 0.03$ increases the relative intensity of the static pressure fluctuation. A value of the accerelation rate $S = 0.01$ do not affect the scaling characteristics of steady isotropic turbulence.

pressure fluctuation for the case of $M = 4$. These static pressure fluctuation values are obtained as spatial root mean square (RMS) values at each time step. As shown in the figure, the time series of the static pressure fluctuation under an acceleration of $S = 0.01$ is very similar to that obtained without acceleration. In contrast, the acceleration of $S = 0.03$ increases the static pressure fluctuation, causing a significant deviation from that of the unaccelerated case. A previous study has used a relative static pressure fluctuation, defined as that normalized using the mean turbulent kinetic energy (Gotoh and Rogallo, 1999), in addition to the RMS of the static pressure fluctuation. Figure 6 (c) and (d) show time series of the instantaneous relative static pressure fluctuation $p^2/[(2/3)\langle k\rangle]^2$ for the case of $M = 4$. Here the denominator is based on the mean turbulent kinetic energy. As shown, the relative static pressure fluctuation under $S = 0.01$ acceleration generally agrees with those obtained without acceleration. On the other hand, in the case of $S = 0.03$ acceleration, the relative static pressure fluctuation deviates significantly from the unaccelerated case and shows significant time variation.

Figure 7 (a) and (b) show RMS values of the static pressure fluctuation as a statistical measure. As shown in the figure, similar to the effects of the acceleration on turbulent kinetic energy and enstrophy, acceleration up to $S = 0.01$ has little to no effect on the rms static pressure fluctuation values. However, acceleration with $S = 0.03$ causes the rms static pressure fluctuation to deviate from the values obtained without acceleration. This deviation increases as M increases, resulting in a smaller spatial scale. Figure 7 (c) and (d) show the RMS of the static pressure fluctuation as a relative value compared to the unaccelerated case. As shown, up to $S = 0.01$, the acceleration does not affect the RMS of the static pressure fluctuation. However, for $S = 0.03$, the relative RMS deviates significantly. This deviation is larger than that observed for turbulent kinetic energy and enstrophy. Therefore, this study considers that this larger deviation indicates that static pressure fluctuation is more sensitive to weak acceleration of the mean flow than turbulent kinetic energy and enstrophy.

Figure 8 (a) and (b) illustrate the effect of acceleration on the relative static pressure fluctuation $\langle p^2\rangle/[(2/3)\langle k\rangle]^2$. In the figure, lines are shown indicating relative static pressure fluctuation intensities of 1 and 0.5. These values are obtained using the joint normal approximation from the autocorrelation function corresponding to the lower and higher Reynolds number conditions (Hinze, 1975). In the absence of the acceleration, the relative static pressure fluctuation intensity under the higher Reynolds number condition is smaller than that under the lower Reynolds number condition and generally falls within the range of these reference values. This result supports the notion that the range of Reynolds numbers set in this study is wide sufficient to change the distribution shape of autocorrelation function of the fluctuations. These figures also confirm that acceleration up to $S = 0.01$ has little effect on the relative static pressure fluctuation intensity. On the other hand, acceleration at $S = 0.03$ increases the relative static pressure fluctuation intensity, especially when the spatial scale of the forcing is small. When the spatial scale is large, the acceleration of $S = 0.03$ may have less effect on the relative static pressure fluctuation intensity.

[DOI: 10.1299/jfst.2025jfst0004]

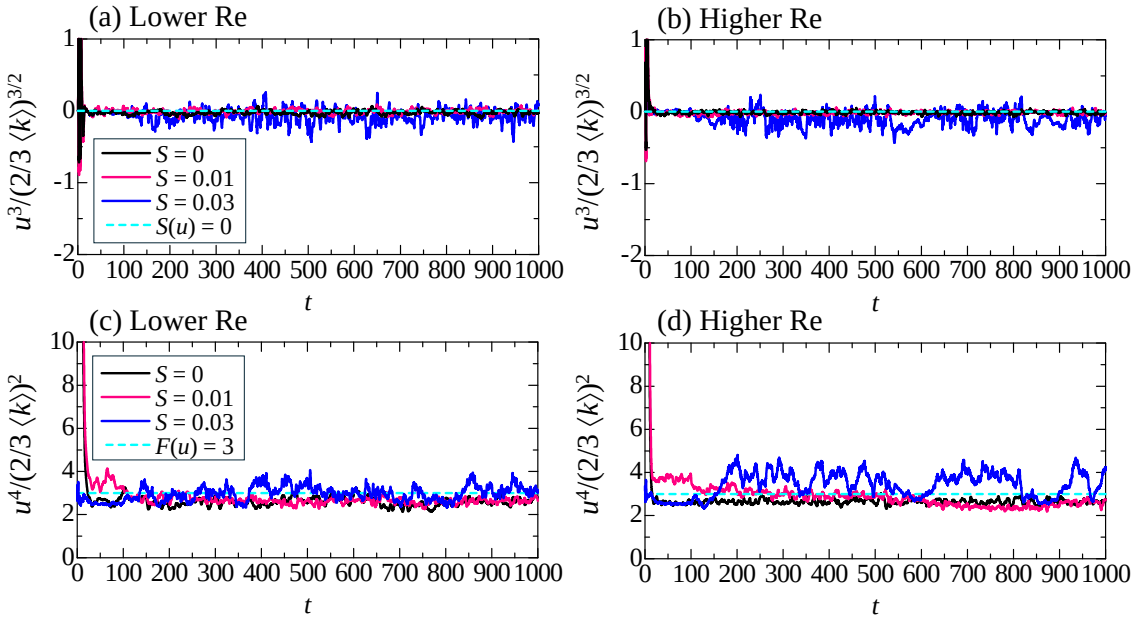

Fig. 9 Time series on instantaneous values of the skewness and flatness values of a velocity fluctuation as a function of the acceleration rate for $M = 4$. For a Gaussian velocity fluctuation the skewness and flatness values are 0 and 3 respectively. The values are obtained as spatial mean at each instant. Without acceleration and at $S = 0.01$, the skewness and flatness values remain around 0 and 3 respectively. For $S = 0.03$, where the acceleration affects the turbulent kinetic energy, the time series shows significant fluctuations over time.

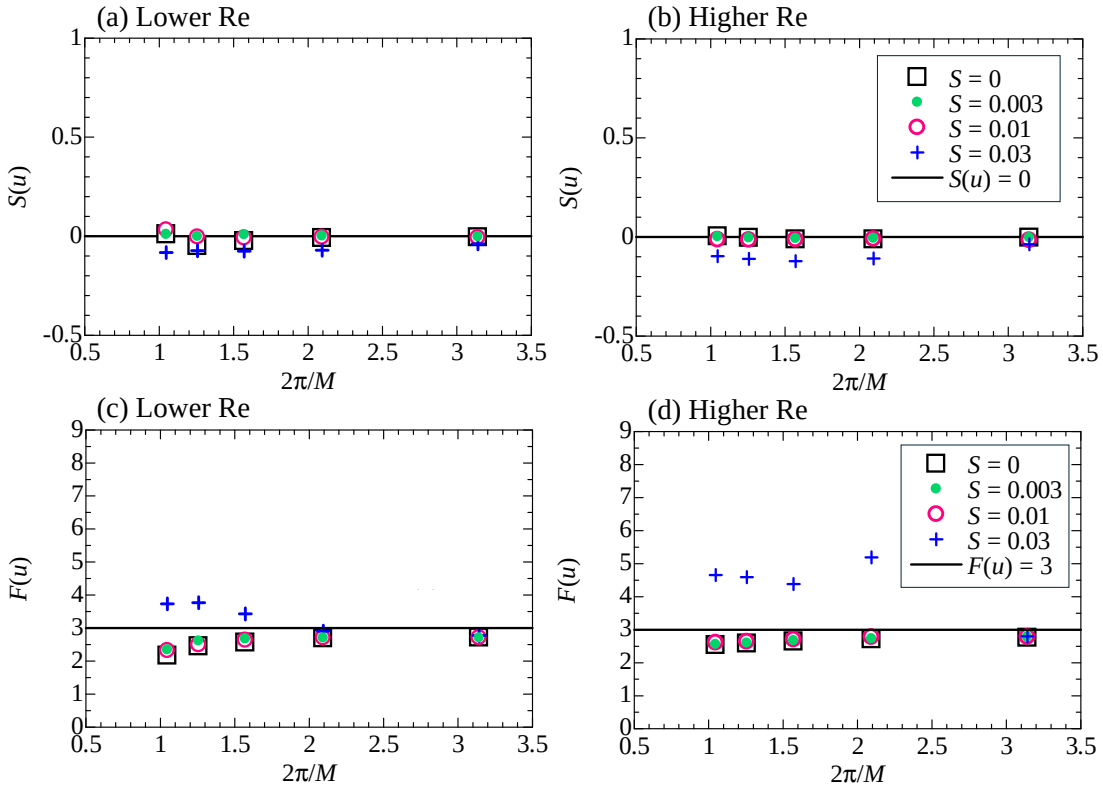

Fig. 10 Mean values of skewness and flatness of velocity fluctuations as a function of $2\pi/M$. For accelerations up to $S = 0.01$, the acceleration does not affect the values of skewness and flatness. At $S = 0.03$ the acceleration affects the flatness. The effect of acceleration on skewness is less pronounced than on flatness value.

[DOI: 10.1299/jfst.2025jfst0004]

Next, this study examines the characteristics of turbulence under acceleration using the skewness and kurtosis of the velocity fluctuations. Skewness and kurtosis are statistical measures obtained by averaging the instantaneous values of skewness and flatness over time, as defined below: $S(u) = u_1^3/\langle u_1^2\rangle^{3/2}$ and $F(u) = u_1^4/\langle u_1^2\rangle^2$, where the denominator of each of these forms is the averaged value, in order to show not only the average value but also the instantaneous value for these factors. Here, skewness and flatness factors are expected to be zero and three, respectively, when a fluctuation follows the Gaussian distribution. Then, the time series of these quantities are shown. Figure 9 (a) and (b) show the time series of instantaneous skewness. The instantaneous skewness values are obtained as spatially averaged values at each instant. As shown in the figures, the instantaneous skewness remains close to zero in both the non-accelerated case and the $S = 0.01$ acceleration case. On the other hand, while the $S = 0.03$ acceleration, which affects the turbulent kinetic energy, seems to have little effect on the average skewness, it does cause the time series of the instantaneous skewness to show fluctuations. These results are observed under both low and high Reynolds number conditions. Figure 9 (c) and (d) show the time series of the instantaneous flatness of the velocity fluctuations within the turbulence. The instantaneous flatness values are also obtained as spatially averaged values at each time step. As shown, the time series of the instantaneous flatness remains around a value of three both in the unaccelerated case and in the case of $S = 0.01$ acceleration, which does not affect the turbulent kinetic energy. However, under the influence of $S = 0.03$ acceleration, similar to the influence on the skewness time series, the instantaneous flatness time series shows fluctuations. In addition, the $S = 0.03$ acceleration seems to cause a slight bias in the flatness values, increasing them slightly above a value of three.

The dependence of mean values of skewness and flatness on spatial scale is shown in the Fig. 10. Mean values of the skewness and flatness are obtained by time averaging the instantaneous skewness and flatness. Figure 10 (a) and (b) illustrate the dependence of skewness on spatial scale. As can be seen in the figures, the skewness values in both the non-accelerated case and with acceleration up to $S = 0.01$ are well aligned to zero. On the other hand, acceleration with $S = 0.03$, which affects the turbulent kinetic energy, can cause the skewness to deviate slightly from zero. The acceleration in this study is applied along the x-axis, so the tendency for the skewness to decrease with acceleration may vary depending on the direction of the applied acceleration. Figure 10 (c) and (d) show the dependence of flatness on spatial scale. As can be seen, the flatness values remain close to three both in the unaccelerated case and at $S = 0.01$ acceleration. However, at $S = 0.03$ acceleration, which affects the turbulent kinetic energy, the flatness can increase as the spatial scale decreases. Since this effect of acceleration on turbulent kinetic energy is observed at smaller spatial scales, the increase in turbulent kinetic energy due to acceleration may be accompanied by an increase in flatness.

4. Conclusion

The aim of this study was to validate a model that quantifies the effect of weak but prolonged mean flow accelerations, such as those encountered during wind tunnel blockage, on the turbulent kinetic energy of the primary turbulence. This model, based on the k-epsilon model, was developed in previous research. To validate this model, this study focused on cases where the turbulence remains steady and isotropic under acceleration. In such cases, modeling suggests that this type of acceleration should have no effect on the turbulent kinetic energy. Our study tested this hypothesis by analyzing turbulence within a periodic box under mean flow acceleration. The analysis was structured using high-order accurate central difference methods and time integration techniques, which are expected to allow quantitative analysis of not only turbulent kinetic energy but also static pressure fluctuation. The effects of this type of acceleration on turbulence were studied as a function of the magnitude of the mean flow acceleration and the spatial scale of the primary turbulence. As a result, when the acceleration rate S is large, the mean flow acceleration causes a significant deviation in the turbulent kinetic energy. In contrast, when the acceleration rate is small, the acceleration has almost no effect on the turbulent kinetic energy, which is consistent with the prediction of the model. It was also confirmed that when the acceleration is small, the enstrophy, the RMS static pressure fluctuation, the relative static pressure fluctuation intensity, higher-order statistics of a velocity fluctuation are largely unaffected by the acceleration.

Acknowledgments

This work was partly supported by the Japanese Ministry of Education, Culture, Sports, Science and Technology through Grants-in-Aid (Nos. 21K03859 and 22H01684). The authors acknowledge the financial support served by Okayama University with the donations from DOWA HOLDINGS Co., Ltd. and TOHO ELECTRIC INDUSTRIAL Co., Ltd. The part of this study was supported by Wesco Scientific Promotion Foundation.

[DOI: 10.1299/jfst.2025jfst0004]

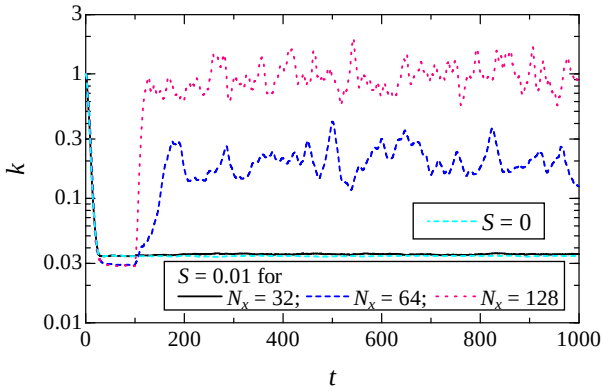

Fig. 11 The effect of the spatial grid resolution N_x on time histories of k with the acceleration is examined. Here, a value of the parameter M is set to 6. The two cases with more grid points are qualitatively different from the case with $N_x = 32$, with the result that the weak acceleration affects the turbulent kinetic energy.

Appendix

This study examined how this discontinuity affects the turbulence statistics by analyzing the grid size dependence of the time history of the turbulent kinetic energy, the primary focus of this study. As illustrated in Fig. 11, this study presents the time history of turbulent kinetic energy for two different grid sizes, focusing on the case of smallest turbulent kinetic energy for $M = 6$. As shown in the figure, for the grid size N_x of 32, the time series data of k for weak acceleration agree well with those for the no-acceleration case, in agreement with our original results, where N_x is a number of grid points for the x direction. In contrast, for the grid sizes of 64 and 128, the time histories of k under the acceleration become significantly larger than those without acceleration. The grid convergence has not been obtained as shown in Fig. 11. The present results should be interpreted with great care. These results suggest that the effects of the discontinuity can be negligible when $N_x = 32$, in contrast to the other two conditions of N_x. The primary reason for the diminished impact is believed to be the reduction in the magnitudes of the longitudinal partial derivatives in Eq. (11), specifically, the decrease in the influence of the discontinuity. This observation suggests difficulties associated with applying direct numerical simulation with Eq. (11) to this problem, which is the main reason for selecting LES analysis in the present investigation instead.

References

Ayyalasomayajula, S. and Warhaft, Z., Nonlinear interactions in strained axisymmetric high-Reynolds-number turbulence, Vol. 566 (2006), pp. 273-307.

Barlow, J. B. and Rae, W., H., Low-Speed Wind Tunnel Testing, third ed., Wiley-Interscience (1999), pp. 665-679.

Choi, C. K. and Kwon, D. K., Wind tunnel blockage effects on aerodynamic behavior of bluff body, Wind and Structures, Vol. 1 (1998), pp. 351-364.

Clay, M. P. and Yeung, P. K., A numerical study of turbulence under temporally evolving axisymmetric contraction and subsequent relaxation, Journal of Fluid Mechanics, Vol. 805 (2016), pp. 460-493.

Comte-Bellot, G. and Corrsin, S., Simple eulerian time correlation of full-and narrow-band velocity signals in grid-generated, 'isotropic' turbulence, Journal of Fluid Mechanics, Vol. 48, No. 2 (1971), pp. 273-337.

de Bruyn Kops, S. M. and Riley, J. J., Direct numerical simulation of laboratory experiments in isotropic turbulence, Physics of Fluids, Vol. 10, No. 9 (1998), pp. 2125-2127.

de Graaff, D. B. and Eaton, J. K., Reynolds-number scaling of the flat-plate turbulent boundary layer, Journal of Fluid Mechanics, Vol. 422 (2000), pp. 319-346.

Girimaji, S. S., Jeong, E. and Poroseva, S. V., Pressure-strain correlation in homogeneous anisotropic turbulence subject to rapid strain-dominated distortion, Physics of Fluids, Vol. 15, No. 10 (2003), pp. 3209-3222.

Gomes-Fernandes, R., Ganapathisubramani, B. and Vassilicos, J. C., Particle image velocimetry study of fractal-generated turbulence, Journal of Fluid Mechanics, Vol. 711 (2012), pp. 306-336.

Goto, S. and Vassilicos, J. C., Energy dissipation and flux laws for unsteady turbulence, Physics Letters A, Vol. 379, No. 16-17 (2015), pp. 1144-1148.

[DOI: 10.1299/jfst.2025jfst0004]

Gotoh, T. and Rogallo, R. S., Intermittency and scaling of pressure at small scales in forced isotropic turbulence, Journal of Fluid Mechanics, Vol. 396 (1999), pp. 257-285.

Gylfason, A. and Warhaft, Z., Effects of axisymmetric strain on a passive scalar field: modelling and experiment, Journal of Fluid Mechanics, Vol. 628 (2009), pp. 339-356.

Hadžić, I., Hanjalić, K. and Laurence, D., Modeling the response of turbulence subjected to cyclic irrotational strain, Physics of Fluids, Vol. 13, No. 6 (2001), pp. 1739-1747.

Hinze, J. O., Turbulence (1975), pp. 305-310, McGraw-Hill.

Hirabayashi, R., Suzuki, H. and Mochizuki, S., LES analysis clarifying the response of static pressure fluctuation characteristics in isotropic/anisotropic steady turbulence field to reducing isotropic small-scale spatial resolution, Journal of Physics: Conference Series, Vol. 2585, No. 1 (2013), DOI: 10.1088/1742-6596/2585/1/012006.

Honda, R., Suzuki, H. and Mochizuki, S., Time-series observation of the effects of kinetic energy conservation error on isotropic and anisotropic steady incompressible turbulence, Journal of Physics: Conference Series, Vol. 1978, No. 1 (2021), DOI: 10.1088/1742-6596/1978/1/012026.

Hunt, J. C.R. and Carruthers, D. J., Rapid distortion theory and the ‘problems’ of turbulence, Journal of Fluid Mechanics, Vol. 212 (1990), pp. 497-532.

Kashiwagi, T., Suzuki, H. and Mochizuki, S., Uncertainty evaluation due to the difference in definitions of the acceleration parameter to examine the influence of mean flow acceleration on the experimental turbulent flows, Journal of Physics: Conference Series, Vol. 2369, No. 1 (2022), DOI: 10.1088/1742-6596/2369/1/012012.

Kobayashi, H., The subgrid-scale models based on coherent structures for rotating homogeneous turbulence and turbulent channel flow, Physics of Fluids, Vol. 17, No. 4 (2005), DOI: 10.1063/1.1874212.

Krogstad, P., Å. and Davidson, P. A., Freely decaying, homogeneous turbulence generated by multi-scale grids, Journal of Fluid Mechanics, Vol. 680 (2011), pp. 417-434.

Kurian T. and Franssons, J. H. M., Grid-generated turbulence revisited, Fluid Dynamcis Research, Vol. 41 (2009), DOI: 10.1088/0169-5983/41/2/021403.

Laneville, A., Turbulence and blockage effects on two dimensional rectangular cylinders, Journal of Wind Engineering and Industrial Aerodyamics, Vol. 33 (1990), pp. 11-20.

Lavoie, P., Djenidi, L. and Antonia, R. A., Effects of initial conditions in decaying turbulence generated by passive grids, Journal of Fluid Mechanics, Vol. 585 (2007), pp. 395-420.

Mohamed, M. S. and LaRue, J. C., The decay power law in grid-generated turbulence, Journal of Fluid Mechanics, Vol. 219 (1990), pp. 195-214.

Morinishi, Y., Lund, T. S., Vasilyev, O. V. and Moin, P., Fully conservative higher order finite difference schemes for incompressible flow, Journal of Computational Physics, Vol. 143, No. 1 (1998), pp. 90-124.

Mugundhan, V., Pugazenthi, R. S., Speirs, N. B., Samtaney, R. and Thoroddsen, S. T., The alignment of vortical structures in turbulent flow through a contraction, Journal of Fluid Mechanics, Vol. 884 (2020), pp. A5-1-39.

Nagata, K., Sakai, Y., Inaba, T., Suzuki, H., Terashima, O. and Suzuki, H., Turbulence structure and turbulence kinetic energy transport in multiscale/fractal-generated turbulence, Physics of Fluids, Vol. 25, No. 6 (2013), DOI: 10.1063/1.4811402.

Örlü, R. and Schlatter, P., Comparison of experiments and simulations for zero pressure gradient turbulent boundary layers at moderate Reynolds numbers, Experiments in Fluids, Vol. 54 (2013), pp. 1-21.

Ota, T., Okamoto, Y. and Yoshikawa, H., A correction formula for wall effects on unsteady forces of two-dimensional bluff bodies, Journal of Fluids Engineering, Vol. 116 (1994), pp. 414-418.

Pope, S. B., Turbulent Flows, Cambridge University Press (2000), pp. 373-404.

Rosales, C. and Meneveau, C., Linear forcing in numerical simulations of isotropic turbulence: Physical space implementations and convergence properties, Physics of fluids, Vol. 17, No. 9 (2005), DOI: 10.1063/1.2047568.

Schlatter, P., Örlü, R., Li, Q., Brethouwer, G., Fransson, J. H. M., Johansson, A. V. and Alfredsson, P. H., Turbulent boundary layers up to Re_θ = 2500 studied through simulation and experiment, Physics of Fluids, Vol. 21 (2009), DOI: 10.1063/1.3139294.

Suzuki, H., Nagata, K., Sakai, Y., Hayase, T., Hasegawa, Y. and Ushijima, T., An attempt to improve accuracy of higher - order statistics and spectra in direct numerical simulation of incompressible wall turbulence by using the compact schemes for viscous terms, International Journal for Numerical Methods in Fluids, Vol. 73, No. 6 (2013a), pp.509-522.

Suzuki, H., Nagata, K., Sakai, Y., Hayase, T., Hasegawa, Y. and Ushijima, T., Direct numerical simulation of fractal-

[DOI: 10.1299/jfst.2025jfst0004]

generated turbulence, Fluid Dynamics Research, Vol. 45, No. 6 (2013b), DOI: 10.1088/0169-5983/45/6/061409.

Suzuki, H., Mochizuki, S. and Hasegawa, Y., Validation scheme for small effect of wind tunnel blockage on decaying grid-generated turbulence, Vol. 11, No. 3 (2016), DOI: 10.1299/jfst.2016jfst0012.

Suzuki, H., Mochizuki, S. and Hasegawa, Y., Numerical-based theoretical analysis on effects of weak fluid acceleration of free-stream due to wind-tunnel blockage on grid-generated turbulence, Vol. 62 (2018), pp. 1-8.

Suzuki, H., Hasebe, K., Hasegawa, Y. and Ushijima, T., Reduced conservation error of kinetic energy using a Runge-Kutta algorithm with reduced numerical dissipation, Journal of Physics: Conference Series, Vol. 1633, No. 1 (2020a), DOI: 10.1088/1742-6596/1633/1/012021.

Suzuki, H., Mochizuki, S. and Hasegawa, Y., Quasi-analytical solutions of a turbulence-modeling equation on the robustness of decaying homogeneous turbulence, Advances in Mechanical Engineering, Vol. 12, No. 2 (2020b), pp. 1-13.

Valente, P. C. and Vassilicos, J. C., Universal dissipation scaling for nonequilibrium turbulence, Physical Review Letters, Vol. 108, No. 21 (2012), DOI: 10.1103/PhysRevLett.108.214503.

Valente, P. C. and Vassilicos, J. C., The decay of turbulence generated by a class of multiscale grids, Journal of Fluid Mechanics, Vol. 687 (2013), pp. 300-340.

Vassilicos, J. C., Dissipation in turbulent flows, Annual Review of Fluid Mechanics, Vol. 47 No. 1 (2015), pp. 95-114.

West, G. S. and Apelt C. J., The effects of tunnel blockage and aspect ratio on the mean flow past a circular cylinder with Reynolds numbers between 10^4 and 10^5, Journal of Fluid Mechanics, Vol. 114 (1982), pp. 361-377.

Zusi, C. J. and Perot J. B., Simulation and modeling of turbulence subjected to a period of uniform plane strain, Physics of Fluids, Vol. 25, No. 11 (2013), DOI: 10.1063/1.4821450.

Zusi, C. J. and Perot J. B., Simulation and modeling of turbulence subjected to a period of axisymmetric contraction or expansion, Physics of Fluids, Vol. 26, No. 11 (2014), DOI: 10.1063/1.4901188.

[DOI: 10.1299/jfst.2025jfst0004]